

A. S. Rawool · Sushanta K. Mitra · S. G. Kandlikar

Numerical simulation of flow through microchannels with designed roughness

Received: 9 September 2005 / Accepted: 5 November 2005 / Published online: 9 December 2005
© Springer-Verlag 2005

Abstract A three-dimensional numerical simulation of flow through serpentine microchannels with designed roughness in form of obstructions placed along the channels walls is conducted here. CFD-ACE+ is used for the numerical simulations. The effect of the roughness height (surface roughness), geometry, Reynolds number on the friction factor is investigated. It is found that the friction factor increases in a nonlinear fashion with the increase in obstruction height. The friction factor is more for rectangular and triangular obstructions and it decreases as the obstruction geometry is changed to trapezoidal. It is observed that the obstruction geometry, i.e., aspect ratio plays an important role in prediction of friction factor in rough channels. It is also found that the pressure drop decreases with the increase in the roughness pitch. Hence, the roughness pitch is an important design parameter for microchannels.

Keywords Microchannel · Numerical · Obstructions
Surface roughness · Pitch

List of symbols

μ	Viscosity of fluid
ρ	Density of fluid
V	Velocity of fluid
P	Pressure
ΔP	Pressure drop between inlet and outlet of serpentine channel
H_{obs}	Height of obstruction

l_1	Streamwise length of obstruction at top
l_2	Streamwise length of obstruction at bottom
L_1	Length of first segment of serpentine channel
L_2	Length of second segment of serpentine channel
L_3	Length of third segment of serpentine channel
Re	Reynolds number
f	Friction factor
p	Pitch of obstructions
W	Base channel width
W_{cf}	Constricted channel width
ε	Mean roughness height

1 Introduction

Microchannels are becoming an integral part of most microfluidic devices. Depending upon the fabrication processes, in most cases, these channels have surface roughness height comparable with the channel dimension. Hence, it is important to understand the flow through these rough channels and compute the friction factors associated with such flows. These will then form the design basis for the microfluidic devices.

Bahrami et al. (2005a) developed an analytical method for estimation of frictional resistance for fully developed laminar flow in rough microchannels based on a Gaussian isotropic distribution for roughness. In their further work (Bahrami et al. 2005b), they have developed an expression for friction factor in microchannels of arbitrary cross-section. The proposed expression is in terms of geometric parameters such as area, perimeter and polar moment of inertia. Kandlikar et al. (2005) have modeled the surface roughness in rectangular minichannels as sawtooth obstruction. They have proposed three new parameters (maximum profile peak height, mean spacing of profile irregularities and floor distance to mean line) to characterize the surface roughness. The Colebrook's relation for friction factor (Colebrook 1939) is modified considering the fact that effective area of flow is decreased when the relative

A. S. Rawool · S. K. Mitra (✉)
Department of Mechanical Engineering,
Indian Institute of Technology Bombay,
Mumbai 400076, India
E-mail: skmitra@me.iitb.ac.in

S. G. Kandlikar
Department of Mechanical Engineering, Rochester Institute
of Technology, Rochester, NY 14623-5603, USA

roughness is more and hence instead of nominal diameter, the constricted flow diameter is used in their calculations. They have modified the Moody diagram (Moody 1944) accordingly for the calculation of friction factor.

Mala and Li (1998) have experimentally investigated water flow through microtubes. They have reported increase in friction factor at higher Reynolds number as compared to conventional flow theory. They have also reported that the friction factor depends on channel material, which signifies the effect of surface characteristics on frictional pressure drop. Koo and Kleinstreuer (2004, 2004) have numerically investigated the effect of surface roughness on microchannel flow. They have used a porous medium layer (PML) to represent the surface roughness. Croce and D'Agaro (2004) have studied the effect of surface roughness on heat transfer using randomly generated peaks with different shapes and distributions. Peng and Peterson (1996) have experimentally investigated convective heat transfer and fluid flow in microchannels. Weilin et al. (2000) have studied flow characteristics in trapezoidal silicon microchannels. They have reported higher frictional pressure drop as compared to conventional theory. Hu et al. (2003) have numerically studied the effect of three-dimensional roughness elements on fluid flow through microchannels. However, they have modeled roughness elements as arrays of square projections mounted on the wall. Schmitt and Kandlikar (2005) have experimentally investigated the effect of repeating microstructures on pressure drop through straight microchannels.

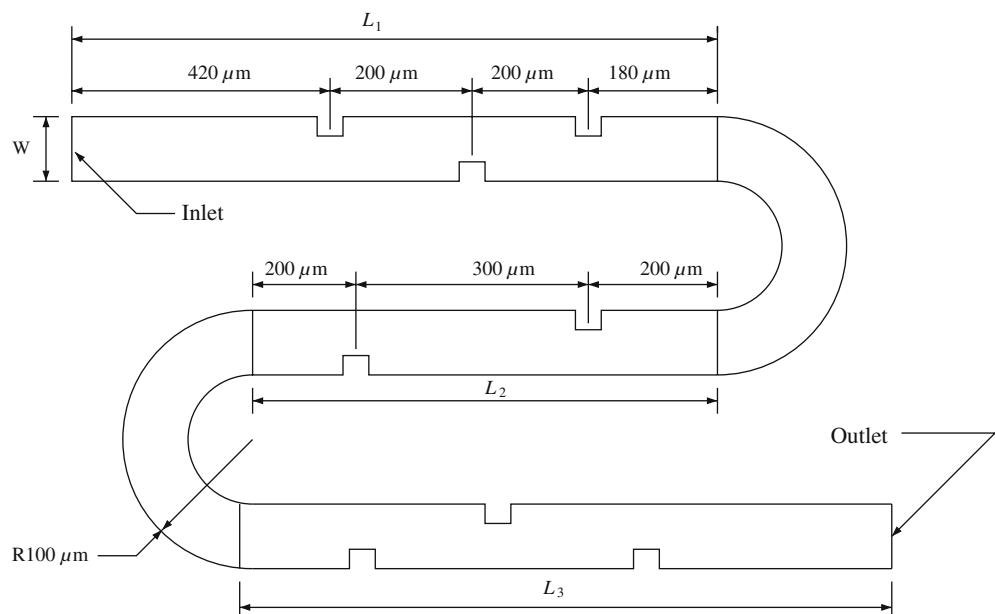
From the available literature, it is observed that modeling attempts have been made to characterize the flow through microchannels with roughness. However, numerical simulation of such channels with random

roughness is extremely difficult. Hence, to investigate the problem numerically, the surface roughness is modeled as regular obstructions placed on the channel walls. The shape of the obstructions is assumed to be trapezoidal, with rectangular and triangular obstructions as extreme cases. This selection of surface roughness elements covers a range of surface roughness patterns observed in actual practice. The pressure drop in microchannels with designed roughness is of interest, as it departs significantly from the pressure drop calculated using classical sudden contraction and expansion correlations (Fox et al. 2001). The effects of various parameters such as Reynolds number, obstruction geometry and height on the friction factor are studied. Moreover the wall roughness is modeled as sawtooth elements, and the effect of pitch of roughness elements on the flow profile and the friction factor is studied.

2 Model for microchannel

A schematic of the channel considered is shown in Fig. 1. The depth of the channel in the direction perpendicular to plane of paper is $100\ \mu\text{m}$. The width of the channel is $100\ \mu\text{m}$. Thus, the channel has a square cross-section of $100\ \mu\text{m}\times 100\ \mu\text{m}$. The channel consists of three straight segments connected by two semicircular arcs. The straight segments have lengths $L_1 = 1,000\ \mu\text{m}$, $L_2 = 700\ \mu\text{m}$ and $L_3 = 1,000\ \mu\text{m}$, and the radius of curvature of the channel axis at the bend is $150\ \mu\text{m}$. Obstructions of various types are placed on the channel walls, perpendicular to the flow direction as shown in Fig. 2. These obstructions are placed in a staggered or an offset manner as depicted in Fig. 1. Figure 2 also

Fig. 1 Schematic of a microchannel with roughness elements



shows the enlarged view of one of the the obstructions. An aspect ratio for the obstruction is defined as

$$A = \frac{l_1}{l_2} \quad (1)$$

which is varied from 1 (for rectangular obstruction) to 0 (for triangular obstruction) to obtain various shapes of obstructions. Here l_1 is the length of obstruction at top and l_2 is the length of obstruction at bottom, as shown in Fig. 2. The height of obstruction is varied from 10 to 50 μm . A normalized height of obstruction is defined as

$$h = \frac{\text{height of obstruction}}{\text{width of the channel}} = \frac{H_{\text{obs}}}{W} \quad (2)$$

which is varied from 0.1 to 0.5. The flow is assumed to be steady with constant properties.

2.1 Governing equations

For three-dimensional flow through microchannels, the governing equations are continuity equation and Navier Stokes equations, respectively:

$$\nabla \cdot V = 0, \quad (3)$$

$$\rho V(\nabla \cdot V) = -\nabla P + \mu \nabla^2 V, \quad (4)$$

where ρ is density of air, V is velocity of air, P is pressure and μ is viscosity of air. For the inlet boundary condition, a constant velocity corresponding to the given Reynolds number is specified at the inlet cross-section. Since this study aims at investigating the effect of various parameters on the friction factor, using a fully developed velocity boundary condition at inlet will not

result in any change in the nature of variation of friction factor with various parameters. Hence constant inlet velocity boundary condition is selected in this study. At outlet, zero gauge pressure is specified. No slip condition is imposed at all other boundaries.

3 Numerical simulation

Commercial CFD code CFD-ACE+ (2002) is used to numerically simulate the flow through the channel. Different obstruction geometries are created and meshed using CFD-GEOM modeler. Unstructured grid using prismatic elements is used for generating mesh. A grid independence study is carried out by varying the number of elements in the domain. The channel with triangular obstructions of maximum height ($A=0$, $h=0.5$) is used for grid independence study. Extra fine mesh with a source of 6×10^{-7} (CFD-ACE+ 2002) is used at the tip of obstructions and other sharp corners as shown in Fig. 3. A grid having 129,248 elements is found to be sufficient as any further refinement does not produce any change in velocity and pressure profiles at various cross-sections. Velocities corresponding to Reynolds number ranging from 40 to 200 are used in the simulation. Upwind scheme is used for velocity calculation. CGS+Pre solver (CFD-ACE+ 2002) is used for velocity, while AMG solver is used for pressure correction. Parametric solver is used to solve for values of velocity corresponding to a range of Reynolds number. A three-dimensional flow simulation over entire length ($L_1 + L_2 + L_3$) (Fig. 1) is carried out. The effect of various parameters such as obstruction height, aspect ratio on friction factor is studied here. For this purpose friction factor is defined as:

$$f = \frac{\Delta P}{\frac{1}{2} \rho V_{\text{inlet}}^2}, \quad (5)$$

where ΔP is measured between inlet and outlet cross-sections of the serpentine channel as shown in Fig. 1.

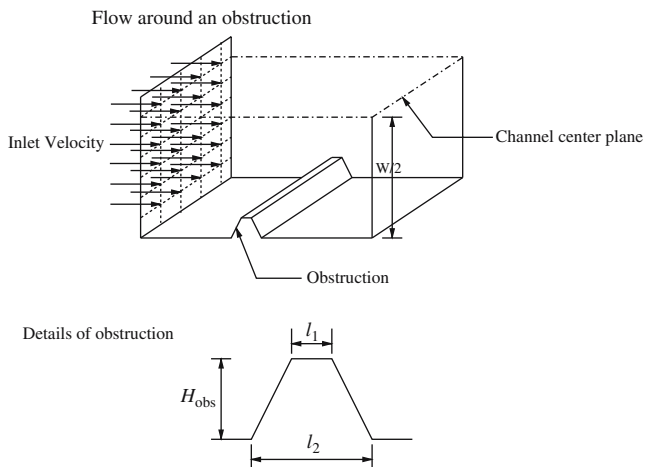


Fig. 2 Geometry of roughness element

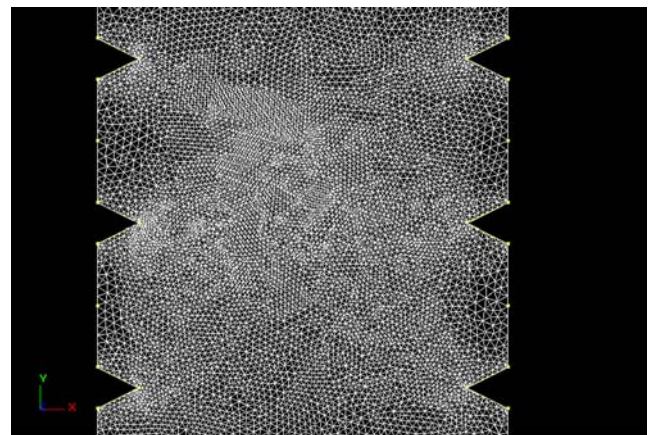


Fig. 3 Details of the mesh used for simulation

4 Results and discussions

Figure 4 shows the enlarged view of flow near one of the obstructions in the serpentine channel, for the case of $Re=200$, $h=0.3$ and $A=0.5$. The plot shows velocity vectors at the midplane section along the depth of the channel. Recirculation of the air in the wake of the obstruction is observed here. Figure 5 shows the velocity magnitude (i.e., square root of summation of squares of three velocity components) plots in various cross-sections along the entire channel length.

The effect of Reynolds number on friction factor is depicted in Fig. 6 for the case of obstruction having $A=0.5$. It is found that the friction factor decreases nonlinearly with the increase in Reynolds number. The variation of friction factor along with Reynolds number is similar for other aspect ratios.

Figures 7, 8 and 9 show the effect of the roughness geometry on the friction factor. It is found that as the obstruction aspect ratio is decreased from $A=1$, the friction factor in the channel decreases. This is because in case of rectangular obstructions, there is a sudden flow in transition from larger area to smaller area, hence the pressure drop is large. With decreasing aspect ratio, the flow transition is more gradual and hence the friction factor decreases with the decrease in aspect ratio. However, for the case of $A=0$ the friction factor is found to be higher than that corresponding to $A=0.25$. This is due to the fact that in case of triangular obstruction, the sharp tip of the roughness element causes a significant flow separation. This flow separation causes additional pressure drop. Hence the friction factor for channel with triangular obstructions is larger as compared to channel with trapezoidal obstruction. It is observed in Figs. 8 and 9 that the increase in friction factor in channels having triangular obstructions becomes less pronounced as the channel height is reduced.

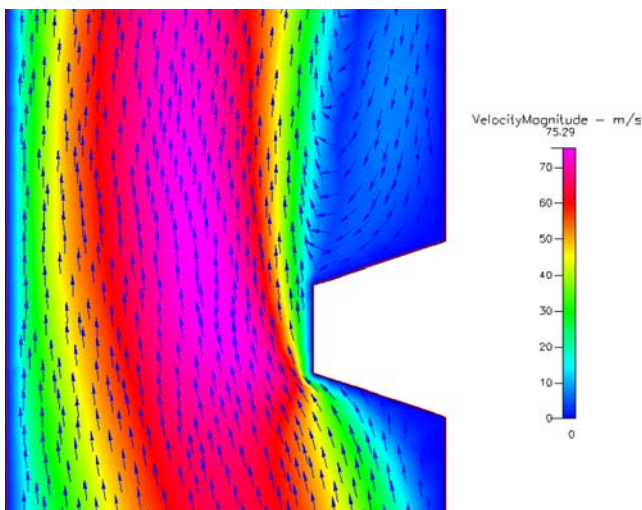


Fig. 4 Enlarged view of velocity vector map around obstruction for $Re=200$, $h=0.3$, $A=0.5$

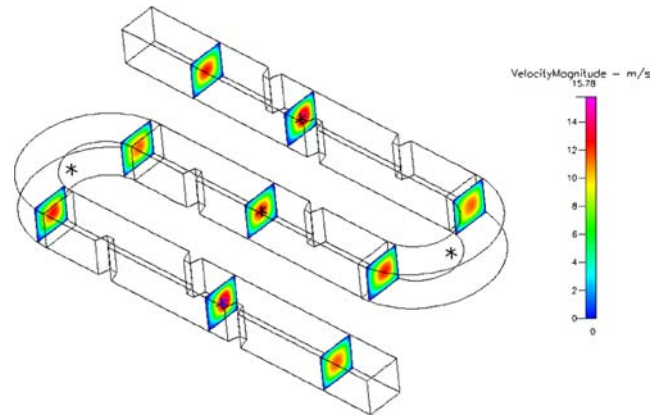


Fig. 5 Velocity magnitude along various cross-sections in the channel

This is because, due to decrease in channel height, the included angle at the obstruction tip increases. This reduces the effect of separation due to sharp tip, which consequently results in reduction of frictional loss. In Fig. 7 it can be observed that the effect of increase in friction factor due to sharp tip of obstruction is less pronounced for low Reynolds number ($Re=40$).

Figure 10 shows the effect of height of the roughness elements on the friction factor in the channel, for various obstruction geometries. It is observed that the increase in friction factor is nonlinear with increasing height of obstruction. Initially the friction factor increases slowly, but as the height of the roughness increases, there is a rapid increase in the friction factor. This is due to the decrease in flow area with the corresponding increase in velocity. The pressure drop across a sudden contraction–expansion is directly

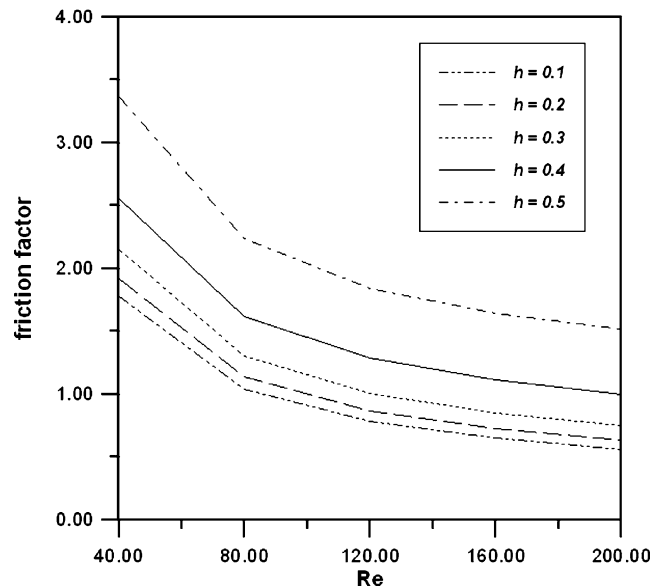


Fig. 6 Variation of friction factor with Reynolds number at $A=0.50$ for different values of h

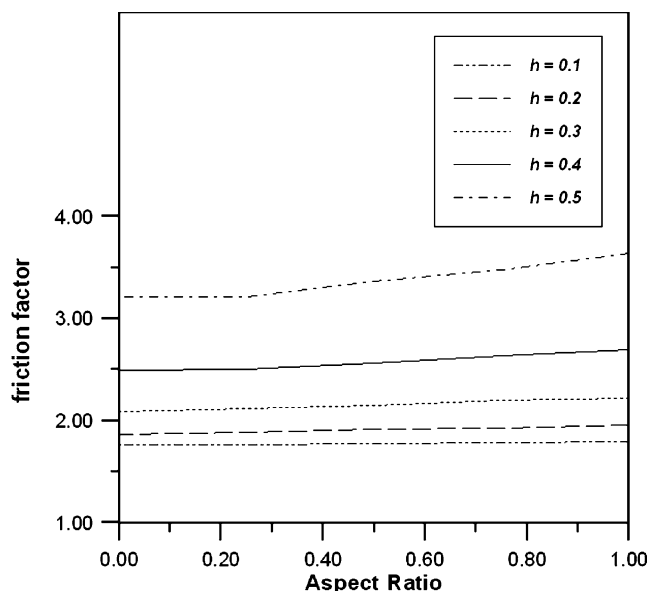


Fig. 7 Variation of friction factor with aspect ratio at $Re=40$ for different values of h

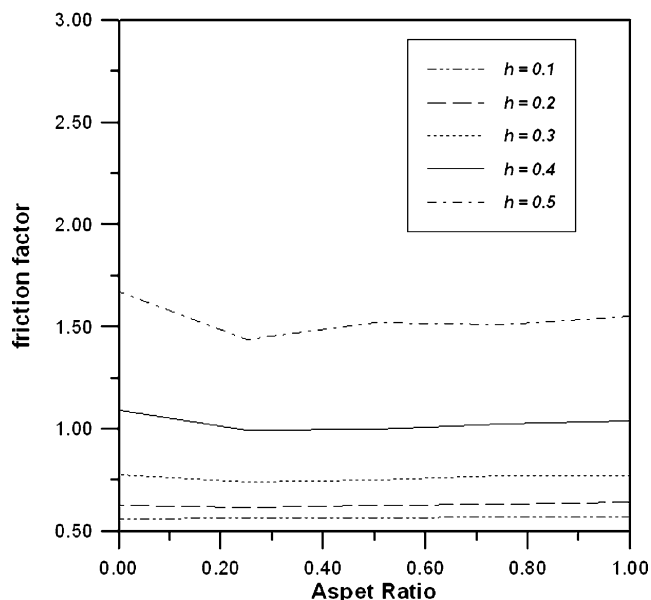


Fig. 9 Variation of friction factor with aspect ratio at $Re=200$ for different values of h

proportional to square of maximum velocity (i.e., the velocity at the obstruction); hence there is a second order increase in the pressure drop with the increase in the height of obstruction. This explains the nonlinear increase in friction factor with channel height. It is also observed that the nature of variation of friction factor with the obstruction height is similar for other values of Reynolds number.

The obstructions of various geometries studied so far can act as surface roughness for microchannels (Kandlikar et al. 2005). To examine the effect of the pitch of

the roughness elements, the surface roughness is modeled as triangular sawtooth obstructions. These obstructions are placed on the channel walls in a non-staggered or aligned way as shown in Fig. 11. To limit the computational time and efforts required, this study is limited to variation of obstruction pitch in a two-dimensional straight channel of length $1,000 \mu\text{m}$. The obstructions considered are having base width $l_2 = 10 \mu\text{m}$, $h = 0.1$ ($H_{\text{obs}} = 10 \mu\text{m}$) and $A = 0$, as shown in Fig. 11. The pitch of obstructions (i.e., the distance between two consecutive obstructions) is varied from 20 to

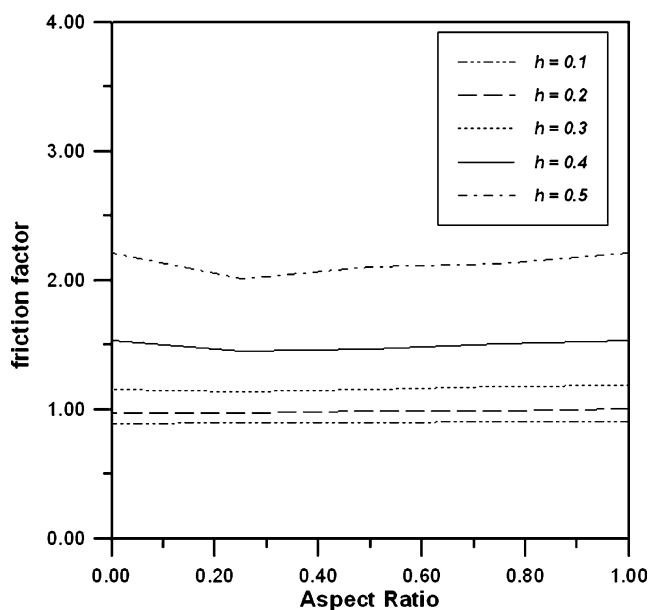


Fig. 8 Variation of friction factor with aspect ratio at $Re=120$ for different values of h

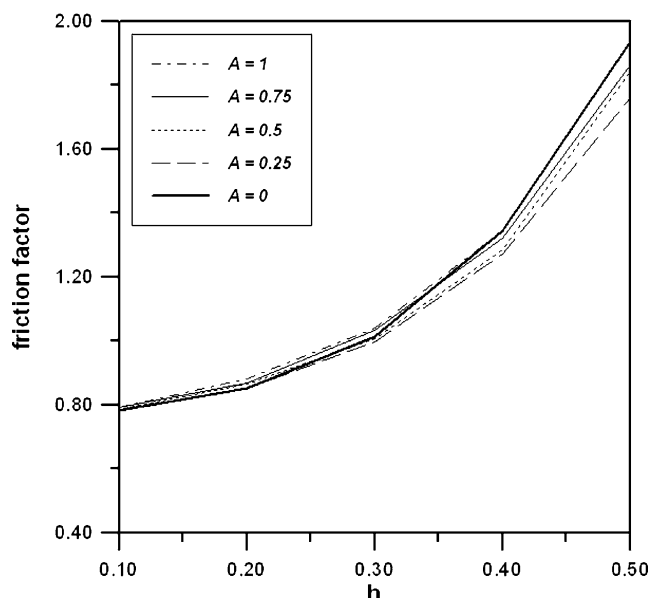


Fig. 10 Variation of friction factor with height of obstruction at $Re=120$ for different values of A

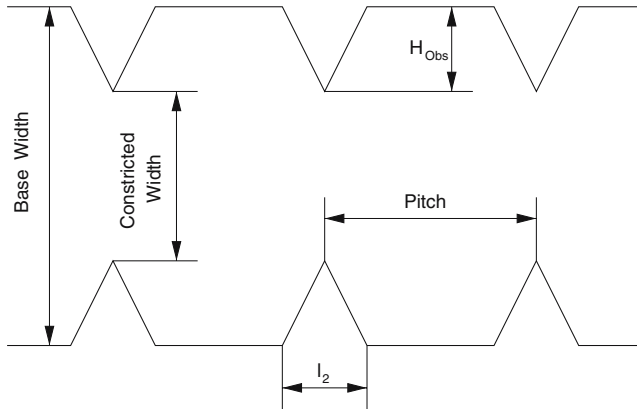


Fig. 11 Channel with triangular surface roughness elements

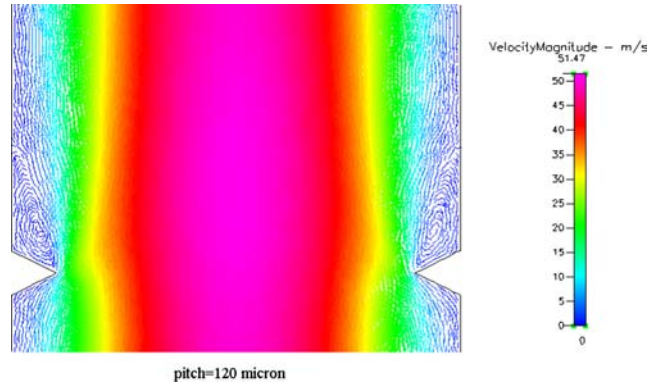


Fig. 13 Velocity vectors in the channel for $p = 120 \mu\text{m}$ at $Re = 100$

150 μm . Figures 12 and 13 show the velocity vectors in the channel at $Re = 100$ for various values of pitch. It is observed that the flow separation takes place at the obstruction. For smaller values of pitch, the flow cannot reattach itself to the walls of the channel as shown in Fig. 12 and hence the effective flow area is significantly lower than the area based on the nominal channel width. It is also found that as the pitch of obstructions is increased, the effective flow area increases, as shown in Fig. 13. The flow gets reattached to the channel wall as the pitch is increased to 100–110 μm .

To analyze the effect of obstruction pitch on pressure drop characteristics, two smooth channels are considered with width equal to base width (100 μm) and constricted width (80 μm), respectively. The use of constricted width is recommended by Kandlikar et al. (2005), which is defined as:

$$W_{cf} = W - 2\epsilon, \tag{6}$$

where ϵ is the height of surface roughness. For the geometry under investigation (Fig. 11) $\epsilon = 10 \mu\text{m}$ and hence the constricted width is 80 μm for this case. The channels considered are straight channels having length equal to 1,000 μm . The pressure drop over these channels is computed for the same value of Reynolds number ($Re = 100$) and is plotted in Fig. 14. It can be seen that

the pressure drop with constricted flow, as proposed by Kandlikar et al. (2005), is significantly higher than the base flow. The simulation result of pressure drop in channels with varying obstruction pitch is also shown in Fig. 14. It is observed that although the height of obstruction is same for all these cases, the pressure drop decreases as the pitch is increased. Thus, roughness pitch is also an important parameter in fluid flow through microchannels and should be taken into account while characterizing microchannels. In this case the pressure drop is measured over a fixed length of the channel (1,000 μm). However, the exit of the channel may contain obstruction element whose position depends on the obstruction pitch. Due to this effect, the variation of pressure drop with obstruction pitch is wavy instead of smooth monotonic variation. It is found that for all values of roughness pitch, the pressure drop in the channel lies between base width and constricted width case.

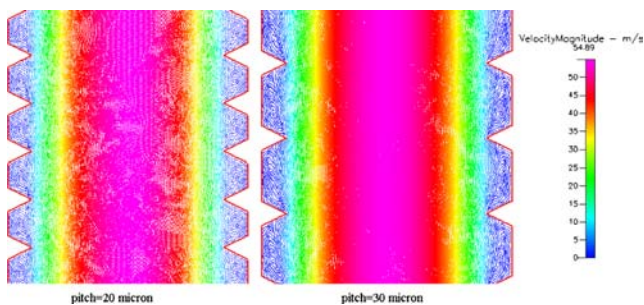


Fig. 12 Velocity vectors in the channel for $p = 20$ and $p = 30 \mu\text{m}$ at $Re = 100$

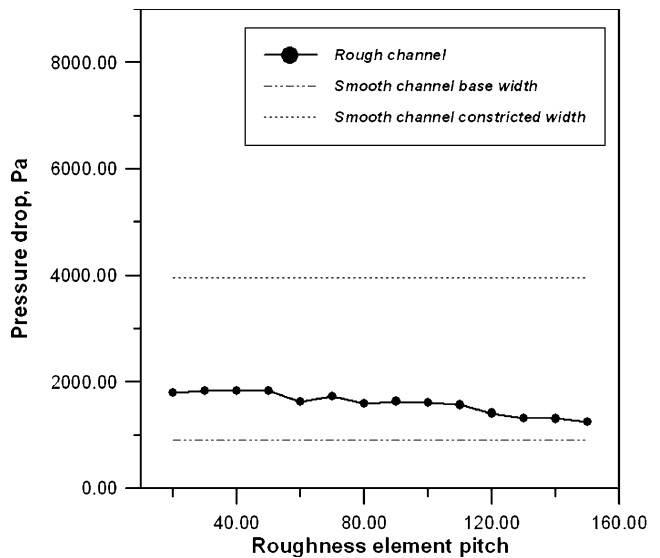


Fig. 14 Variation of pressure drop with pitch of obstructions for $Re = 100$, $h = 0.1$ and $A = 0$

It is also found that the pressure drop for smaller pitch ($\sim 20 \mu\text{m}$) is large compared to higher values of pitch ($\sim 150 \mu\text{m}$). Such behavior can be explained by referring to Figs. 12 and 13. As observed in these figures, for smaller values of pitch, the flow does not reattach itself to the channel wall. Furthermore the number of obstructions in a given length of channel is more for smaller values of pitch. Due to these factors the pressure drop is higher for small value of pitch and it decreases as the obstruction pitch is increased.

It is to be noted that in case of channels with surface roughness, Kandlikar et al. (2005) proposed the use of constricted flow width for estimation of pressure drop. This approach is quite valid provided that the roughness elements are closely spaced. As shown in Fig. 14, it is observed that for higher values of roughness pitch, the pressure drop is closer to the value calculated using base width. For all values of roughness pitch, the pressure drop lies between the limits of base and constricted width.

5 Conclusions

A numerical simulation of flow through microchannels with obstructions placed along the channels walls is conducted in this paper. The effect of various parameters like obstruction height, geometry and Reynolds number on the friction factor is investigated here. It is observed that recirculation zones are created downstream of these obstructions and the friction factor in the channel increases in a nonlinear fashion with the increase in obstruction height. The friction factor is higher for rectangular and triangular obstructions, and it decreases as the geometry is changed to a trapezoidal shape. The friction factor also decreases nonlinearly with the increase in Reynolds number. The surface roughness of the channel wall is modeled as triangular obstructions and the effect of obstruction pitch on the pressure drop is also studied here. It is observed that the pressure drop in rough channel lies between the pressure drop for channel with base width and constricted width. It is found that the pressure drop decreases with the increase in the obstruction

pitch. Hence, the roughness pitch is an important parameter for microchannel flows.

Acknowledgments The support from Suman Mashruwala μ Engineering Laboratory, IIT Bombay, for this work is appreciated.

References

- Bahrami M, Yovanovich MM, Culham JR (2005a) Pressure drop of fully developed, laminar flow in rough microtubes. In: Proceedings of 3rd international conference on microchannels and minichannels, Toronto, Canada
- Bahrami M, Yovanovich MM, Culham JR (2005b) Pressure drop of fully developed, laminar flow in microchannels of arbitrary cross section. In: Proceedings of 3rd international conference on microchannels and minichannels, Toronto, Canada
- CFD-ACE+ software manuals, CFD Research Corporation (2002)
- Colebrook FC (1939) Turbulent flow in pipes, with particular reference to the transition region between the smooth and rough pipe laws. *J Instit Civil Eng Lond* 11:133–156
- Croce G, D'Agaro P (2004) Numerical analysis of roughness effect on microtube heat transfer. *Superlattice Microst* 35:601–606
- Fox RW, McDonald AT, Pritchard PJ (2001) Introduction to fluid mechanics. Wiley, New York
- Hu Y, Werner C, Li D (2003) Influence of three-dimensional roughness on pressure driven flow through microchannels. *Int J Heat Mass Transfer* 125:871–879
- Kandlikar SG, Schmitt DJ, Carrano AL, Taylor JB (2005) Characterization of surface roughness effects on pressure drop in single-phase flow in minichannels. *Phys Fluids* 17
- Kleinstruer C, Koo J (2004) Computational analysis of wall roughness effects for liquid flow in micro-conduits. *ASME J Fluid Eng* 126:1–9
- Kleinstruer C, Koo J (2004) Computational analysis of wall roughness effects on heat transfer in microconduits. *Int J Heat Mass Transfer* 48:2625–2634
- Mala DM, Li D (1998) Flow characteristics of water in microtubes. *Int J Heat Fluid Flow* 20:142–148
- Moody LF (1944) Friction factor for pipe flow. *ASME Trans* 66:671–683
- Peng XF, Peterson GP (1996) Convective heat transfer and flow friction for water flow in microchannel structures. *Int J Heat Mass Transfer* 39:2599–2608
- Schmitt DJ, Kandlikar SG (2005) Effects of repeating microstructures on pressure drop in rectangular minichannels. In: Proceedings of 3rd international conference on microchannels and minichannels, Toronto, Canada
- Weilin Q, Mala M, Li D (2000) Pressure driven water flows in trapezoidal silicon microchannels. *Int J Heat Mass Transfer* 43:353–364